Catalysis Science & Technology

ROYAL SOCIETY OF CHEMISTRY

PAPER

View Article Online
View Journal | View Issue

Cite this: *Catal. Sci. Technol.*, 2025, 15, 3149

Bifunctional Rh/Al-SBA-15 catalysed cascade hydroformylation and hydroxyalkylation of alkenes to fuel precursors†

Krishnan Ravi, [abc] Hanuman Kachgunde,[ab] Venkata D. B. C. Dasireddy, [d] Jim Mensah,[d] Adam F. Lee, *[d] Ankush V. Biradar *[ab] and Karen Wilson *[d]

Received 13th February 2025,
Accepted 19th March 2025

DOI: 10.1039/d5cy00171d

rsc.li/catalysis

Decarbonisation of hard-to-abate liquid transport fuels, notably used in the aviation and shipping sectors, requires new catalytic routes to valorise waste feedstocks. Here we report a bifunctional Rh/Al-SBA-15 catalyst for the one-pot, two step cascade hydroformylation of 1-alkenes with CO/H_2 to form linear and branched aldehydes, and their subsequent hydroxyalkylation (HAA) with 2-methylfuran to form oxygenated jet fuel precursors. A strong synergy between Rh and Al-SBA-15 is observed for hydroformylation, with the bifunctional catalyst significantly more active than Rh/SBA-15 for the first step of the cascade. Superior yields of desired HAA products are observed over Rh/Al-SBA-15 relative to a physical mixture of Rh/SBA-15 and Al-SBA-15. Under syngas (CO/H_2) at 30 bar and 80 °C, alkenes undergo Rh catalysed hydroformylation to aldehydes, and in a subsequent step under N_2, HAA of aldehydes over the solid acid sites of Al-SBA-15 gives an overall ~60% yield of fuel range precursors.

1. Introduction

Climate change associated with fossil fuel combustion, and resulting CO_2 emissions, are driving demand for renewable liquid fuels.[1,2] Such liquid fuels are critical to decarbonise hard-to-abate aviation, marine, agriculture and haulage sectors, and can be sustainably sourced from waste biomass[3] or even CO_2. The molecular and combustion properties of synthetic fuels are determined by both the feedstock and chemical transformation route adopted.[4] Olefin-enriched liquid hydrocarbons can be sourced from biogas *via* Fischer–Tropsch synthesis, and can be upgraded to oxygenates by hydroformylation (wherein olefins are reacted with CO and H_2 to form aldehydes).[5] Hydroformylation of olefins obtained from the pyrolysis of waste plastics is reported,[6] and could be adopted to produce aldehydes *in situ* from alkenes derived by bio-alcohol dehydration,[7] fatty acid decarboxylation[8] or MSW pyrolysis.[9]

Hydroformylation is an atom-efficient commercial process employing Rh or Co metal organometallic catalysts to selectively produce carbonyl compounds on an industrial scale;[5] >10 M tons of aldehyde are produced annually by this route for pharmaceutical and fragrance applications.[10] However, such organometallic catalysts hinder product separation and result in loss of the Rh precious metal industrially favoured for its performance under milder reaction conditions. Heterogenous catalysts for hydroformylation are desirable to improve process intensification, and examples include supported Rh single atoms or nanoparticles, or tethered organometallic complexes.[11] Oxide (*e.g.* Al_2O_3,[12] SiO_2,[13] ZnO,[14] or CeO_2 (ref. 15)), reduced graphene oxide,[16] metal–organic framework,[17] and hydrotalcite[18] supports have been exploited for Rh nanoparticles, and silica grafted 3-diphenyl-phosphinopropyl-triethoxysilane (DPPPTS) tethers[19] or porous organic polymers functionalised with 1,2-bis-(diphenyl-phosphino) ethane[20] to immobilise Rh complexes or Xanthos[21] ligands. However, there are few studies exploring the impact of support acidity: $Rh/H_3PW_{12}O_{40}$ and alkali-exchanged analogues are active for styrene hydroformylation at 80–120 °C and 20 bar CO/H_2 with Cs variants most promising,[22] while doping of $Rh(DPPPTS)/SiO_2$ with AlO_x (from wet impregnation with $Al(NO_3)_3{\cdot}9H_2O$) increased activity for ethylene hydroformylation four-fold by tuning the P-ligand electron density.[23] Although judicious ligand selection can

[a] *Inorganic Materials and Catalysis Division, CSIR-Central Salt & Marine Chemicals Research Institute, G. B. Marg, Bhavnagar-364 002, Gujarat, India. E-mail: ankush@csmcri.res.in*
[b] *Academy of Scientific & Innovative Research (AcSIR), Ghaziabad-201 002, India*
[c] *School of Science, RMIT University, 124 La Trobe Street, Melbourne, VIC 3000, Australia*
[d] *Centre for Catalysis and Clean Energy, School of Environment and Science, Griffith University, Queensland 4222, Australia. E-mail: adam.lee@griffith.edu.au, karen.wilson6@griffith.edu.au*

† Electronic supplementary information (ESI) available: ESI containing experimental details, materials characterisation and catalytic data. See DOI: https://doi.org/10.1039/d5cy00171d

improve the hydroformylation regioselectivity of organometallic complexes, such catalysts are prone to deactivation during thermal regeneration of spent catalysts.

Production of diesel and aviation fuel precursors requires C_{15}–C_{21} and C_8–C_{16} hydrocarbons respectively, and hence chain growth of aldehydes typically obtained by hydroformylation. Chain growth strategies include aldol condensation,[24] hydroxyalkylation–alkylation (HAA),[25] and pinacol coupling.[26] Various homogeneous and heterogeneous Brønsted acid catalysts are also reported for producing oxygenated fuel precursors by condensation of carbonyls with biomass-derived furanics such as 2-methylfuran (2-MF), including phosphotungstic acid,[27] sulfonic acid functionalised carbons,[28–30] polymers,[31] and doped zirconias.[32] Al-SBA-15 is a versatile mesoporous solid acid that is active for HAA[33] and readily doped with metal nanoparticles to create bifunctional catalysts.[34,35] Cascade hydroformylation–acetalization of 1-hexene is reported over weakly acidic Rh/SiO_2,[13] but to our knowledge such bifunctional catalysts have not been exploited in HAA cascades.

We recently reported the cascade hydroformylation–HAA of olefins and 2-MF (Scheme 1) catalysed by homogeneous Rh complexes and solid acids to synthesise fuel precursors.[36] However, the use of soluble Rh species hinders catalyst recycling and continuous operation. Here we report a bifunctional, mesoporous solid acid supported Rh catalyst for the one-pot hydroformylation of olefins under a syngas atmosphere at 80 °C, followed by HAA of the resulting aldehyde products with 2-MF under a N_2 atmosphere at 60 °C.[37] By using a one-pot, two step approach with a gas purge to remove syngas mid-way through the reaction, ~60% oxygenated fuel range precursors are obtained using fully heterogeneous a 2.6 wt% Rh/Al-SBA-15 catalyst.

2. Experimental

2.1 Catalyst synthesis

Support synthesis. Al-SBA-15 with a 5 : 1 Si : Al ratio was synthesized using tetraethyl orthosilicate (TEOS) and aluminium nitrate nonahydrate ($Al(NO_3)_3{\cdot}9H_2O$) as silica and aluminium precursors, respectively. In a typical procedure for Al-SBA-15, 2 g of P123 triblock copolymer template was dissolved in 12 mL of concentrated HCl and stirred in a 250 mL polypropylene bottle until a clear solution was formed. 1.455 g of $Al(NO_3)_3{\cdot}9H_2O$ and 50 mL of deionized water were added and stirred at 45 °C for 30 min (300 rpm). 4.2 mL of TEOS was then added dropwise to the above solution which was subsequently aged at 45 °C for 6 h in an oil bath. Aqueous ammonia was added gradually to adjust the pH to 7, and aging was continued for a further 18 h. The resulting material was aged at 80 °C for another 24 h under static conditions in a hot air oven. The resultant solid was centrifuged, washed, and dried at 70 °C overnight, after which the white solid material was calcined at 550 °C for 5 h. The weight of the solid material after calcination was approximately 1.4 g and was denoted as Al-SBA-15. SBA-15 was synthesised using the same procedure, but with the omission of $Al(NO_3)_3{\cdot}9H_2O$.

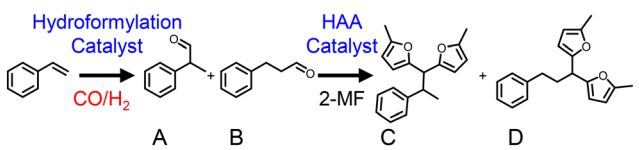

Scheme 1 Synthesis of fuel precursors illustrated for styrene hydroformylation and subsequent HAA of aldehyde intermediates with 2-methyl furan (2-MF).

Synthesis of Rh/Al-SBA-15. Rh/Al-SBA-15 was prepared by impregnating Rh ($RhCl_3{\cdot}XH_2O$, 38–40% Rh) on the mesoporous support using the deposition–precipitation method. The typical synthesis procedures for the catalytic materials are as follows: 0.2 g of Al-SBA-15 was added to 10 mL of deionized water under constant stirring at room temperature. After stirring for 1 h, an appropriate amount of $RhCl_3$ with 0.2 mL of concentrated HCl (corresponding to desired Rh loading of 2 wt%) was added to the mixture/suspension and stirred overnight (12 h) at room temperature. Next, 0.1 M NaOH was slowly added to the reaction mixture to adjust pH of the solution to ~ 9.5, and the resulting mixture was stirred for 1 h. The resultant solid was centrifuged, washed, and dried at 70 °C overnight. The light yellowish solid material obtained was again calcined at 550 °C for 5 h. Rh/SBA-15 was prepared following the same protocol, with the overall process for catalyst synthesis summarised in Fig. S1.†

2.2 Catalyst characterisation

N_2 porosimetry was conducted at 77 K using a Micromeritics ASAP-2010 instrument to measure the N_2 adsorption–desorption isotherm and Brunauer–Emmett–Teller (BET) surface area of the prepared materials. The samples were degassed under vacuum at 200 °C for 3 h before measurements to expel the interlayer water molecules. The NLDFT adsorption model for cylindrical pores was applied to calculate the pore-size distribution of the materials. High-resolution Transmission Electron Microscopy (HR-TEM) images were recorded on a JEOL JEM-2100 electron microscope with an acceleration voltage of 200 kV. Samples for TEM analysis were prepared by loading a small amount of diluted dispersed material onto a lacey-carbon-coated copper grid (300 mesh). Sample-loaded TEM grids were dried for 24 h before analysis. The bright field (BF) detector was applied to capture the TEM micrographs at different magnification to observe the morphology, crystal structure and arrangement of silica and Rh nanoparticles. The morphology of the synthesized catalyst was also obtained by Scanning Electron Microscopy (SEM) which was recorded on a JEOL JSM 7100F microscope, using an accelerating voltage of 18 kV and a probe current of 102 A. Samples were prepared by dispersing

in isopropyl alcohol (IPA), and a drop of the suspension added to the SEM copper grid. Thermogravimetric analysis (TGA) was carried out in Mettler Toledo TGA/SDTA 851e, using a temperature programming from 30 °C to 800 °C at a heating rate of 10 °C min^{-1} in air flowing flow rate of 50 mL min^{-1} and the data were processed using STARe software. Powder X-ray diffraction (XRD) data was obtained using a PANalytical Empyrean (PIXcel 3D detector) system equipped with Cu K_α (λ = 1.54 Å) radiation. The operating voltage and current were 40 kV and 30 mA, respectively. A step size of 0.04° with a step time of 2 seconds was used for data collection. Small angle X-ray was performed on a Xenocs Xeuss 2.0 system equipped with a Cu K_α X-ray source and fixed Pilatus 100k detector, with measurements made over the angular range 2θ = 0.05–5°. The unit cell parameter (a) was calculated for the 100 Bragg peak using the following equations: $d = 0.154\frac{\sqrt{h^2+k^2+l^2}}{2\sin\theta}$ and $a_{100} = 2d_{100}/\sqrt{3}$. FTIR analysis of the samples was recorded on self-supporting wafers prepared as KBr pellets using a Perkin-Elmer GX FTIR spectrometer in the region of 400–4000 cm^{-1} with KBr in a 1 : 20 weight ratio. X-ray photoelectron spectroscopy (XPS) measurements were performed on a Thermo Fisher Nexsa spectrometer equipped with monochromatic Al K_α radiation of energy 1486.6 eV. The pass energy for survey spectra was 200 eV and for high-resolution spectra was set at 50 eV. Dual-beam charge neutralization was used for both low-energy electrons and ions. The sample was at 90° to the analyzer. Core-level spectra were energy referenced to the C 1s binding energy at 284.8 eV; spectral fitting was performed using CASA XPS (v2.3.1.17).

2.3 Hydroformylation/hydroxyalkylation

Hydroformylation was initially performed using styrene as a model substrate, followed by HAA using 2-methyl furan (2-MF). The reaction was carried out in a 50 mL Parr reactor equipped with a thermocouple and overhead stirred. In a typical experiment, 2.4 mmol (0.25 g) of styrene, the required mass of Rh/Al-SBA-15, and 0.25 mL tetradecane internal standard, were added to the reactor with 16 mL of solvent (typically toluene or 2-MF). The reactor was charged, purged of air, and then filled with CO/H_2 (1 : 1 vol ratio) to the desired pressure. Finally, the reactor was heated to the desired temperature under stirring for between 6–9 h. Aliquots of the reaction mixture were collected, diluted with solvent, and analysed using a Shimadzu QP-2010 GC-MS, with a HP-5 (5% diphenyl and 95% dimethyl polysiloxane capillary phase) column, and He as the carrier gas. Conversion and selectivity were determined by quantification of reactant and product peak areas from GC-MS and ^{13}C NMR. Errors in catalytic results were assessed based on repeat experiments (Table S1†) which were ±2%, evidencing a high degree of reproducibility.

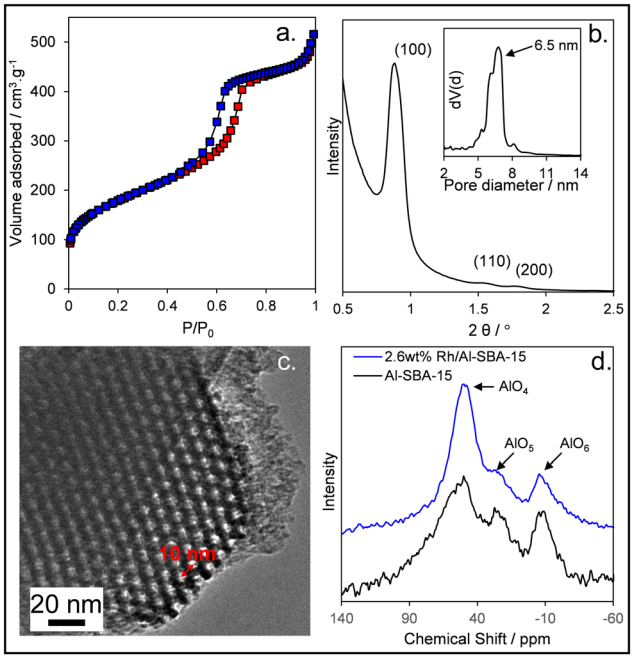

Fig. 1 a) N_2 adsorption–desorption isotherm b) SAXS and (inset) NLDFT pore size distribution from desorption branch of N_2 isotherm and c) TEM of Al-SBA-15(5); d) ^{27}Al MAS-NMR of Al-SBA-15 and Rh doped variant.

3. Results & discussion

3.1 Catalyst characterisation

Successful synthesis of Al-SBA-15 and Rh/Al-SBA-15 (by deposition–precipitation of $RhCl_3$ and subsequent 550 °C calcination) was confirmed by bulk and surface analysis (Fig. 1 and S2–S4†). FE-SEM of the parent Al-SBA-15 revealed the expected alfalfa morphology with fused particles each ~1 μm long and 0.3 μm diameter (Fig. S2†). Nitrogen physisorption measurements were consistent with a type IV isotherm and type I hysteresis loop (Fig. 1a) evidencing close-packed cylindrical mesopores,[38] with a BET surface area of 629 $m^2\ g^{-1}$ (Table 1).

SAXS measurements and calculation of the pore size distribution by NLDFT analysis of the N_2 adsorption isotherm (Fig. 1b and inset respectively) identified ordered mesopores. Calculated values of d_{100} and a_{100} were 10 and 11.5 nm respectively from the (100) Bragg reflection in SAXS, with a mesopore diameter of 6.5 nm determined from NLDFT analysis, in accordance with the ordered, hexagonal mesostructure with 10 nm pore channel spacing seen by HRTEM (Fig. 1c and S2b†) and literature reports.[39] The Si : Al atomic ratio was ~5 from bulk and surface elemental analysis (Fig. S2c†), resulting in an acid loading of 1.2 mmol g^{-1} from NH_3 TPD (Table 1).

The morphology of Rh/Al-SBA-15 was identical to that of the parent Al-SBA-15 (Fig. S3a–c† and Table 1) with solid acidity unaffected by Rh modification and HRTEM revealing ordered pores are retained. No crystalline Al_2O_3 phases were observed by XRD in either Al-SBA-15 or Rh/Al-SBA-15 (Fig.

Table 1 Physical and textural properties of as Al-SBA-15(5) and Rh/AlSBA-15(5)

Catalyst	Bulk Rh content[a]/at%	Surface Rh content[b]/at%	Bulk Si : Al[a]	Surface Si : Al[b]	BET surface area[c]/m^2 g^{-1}	Pore volume[c]/cm^3 g^{-1}	Acid site loading[d]/mmol g^{-1}
Al-SBA-15	—	—	5.3	4	629	0.84	1.24
2.6 wt% Rh/AlSBA-15	0.49	1.2	5.1	4.9	274	1.2	1.22

[a] EDX. [b] XPS. [c] N_2 porosimetry. [d] NH_3 TPD.

S3d†), evidencing successful incorporation of the majority of Al atoms into the silica framework.[40] Although Fig. S3c† shows some 10–20 nm features within the Al-SBA-15 pores indicative of incorporated Rh, the absence of any crystalline Rh phases in powder XRD suggests that most Rh is dispersed in <2 nm particles throughout channels in the mixed oxide support at a bulk loading of 2.6 wt% (by EDX). Tetra-, penta-, and octahedral coordinated Al species were observed by ^{27}Al-MAS-NMR in both samples (Fig. 1d), attributed to framework AlO_4, $AlO_4(OH)$ and some extra framework AlO_6, respectively.[41] This extra-framework AlO_6 may arise from some deposition of AlO_x species which are not detected by powder XRD due to small cluster size and low crystallinity. In the case of Rh/Al-SBA-15, a significant increase in AlO_4 *versus* pentahedral and octahedral Al^{3+} species was observed compared to the parent Al-SBA-15, suggesting perturbation of surface Al species on Rh coordination.

The high resolution Rh 3d XP spectrum of Rh/Al-SBA-15 (Fig. S4a†) exhibited a broad spin–orbit split doublet with $3d_{5/2}$ binding energy (BE) of 308.2 eV. The fitted spectrum of Rh/Al-SBA-15 exhibits ~12% Rh^0 (at 307.3 eV BE) and ~88% Rh^{3+} (at 308.4 eV BE), the former consistent with a metallic core and the latter to an encapsulating Rh_2O_3 layer.[42–44] Quantitative analysis of the Rh metal attenuation (assuming an inelastic mean free path of Rh 3d photoelectrons of 0.6 nm) by an encapsulating oxide matrix suggests a Rh_2O_3 layer of ~0.73 nm (2 monolayers) thick. Note that Rh_2O_3 reduction is facile (<1 min) at 50 °C under a 1% H_2/Ar atmosphere,[45] hence we expect rapid removal of this encapsulating oxide under our reaction conditions. Corresponding Al and Si 2p XP spectra (Fig. S4b and c†) revealed Al^{3+} and Si^{4+} species with $2p_{3/2}$ BEs of 74.7 eV and 103.1 eV, consistent with AlO_x and SiO_x environments in aluminosilicates.[46] The O 1s spectrum of Rh/Al-SBA-15 (Fig. S4d†) exhibited two oxygen species at 532.4 and 531.4 eV, respectively assigned to Si–O–Si(Al) in the aluminosilicate framework and surface hydroxyls.[47]

3.2 Hydroformylation/HAA catalyst activity

The catalytic performance of Rh/Al-SBA-15 and Al-SBA-15 were subsequently assessed for each step in the cascade hydroformylation of styrene under a CO/H_2 atmosphere was first studied at 30–80 °C and 10–40 bar over 2.6 wt% Rh/Al-SBA-15 in tetrahydrofuran (THF) or toluene solvents (Scheme S1 and Table S2†). Toluene favoured higher (98%) conversion and selectivity (90%) to 2-phenylpropanal (**A**) and 3-phenylpropanal (**B**) after 6 h reaction, with the latter product typically dominant.

Temperatures >60 °C and pressures >20 bar offered the highest aldehyde yields, with the linear aldehyde only favoured at 10 bar. Similar pressure dependent selectivity over Rh complexes is attributed branched alkyl–Rh intermediates being stabilised by CO coordination at higher pressure.[48] The hydroformylation performance of 2.6 wt% Rh-Al-SBA-15 compares favourably with 1 wt% Rh/Al_2O_3; the latter requires elevated pressure of (80 bar) $CO:H_2$ to achieve near a near quantitative yield of aldehyde.[12] Although <1.8 nm alumina supported Rh clusters are reportedly efficient for hydroformylation, they are also prone to leaching.[49]

Hydroxyalkylation–alkylation of benzaldehyde with 2-MF was negligible without a solid acid present or at 50 °C over Al-SBA-15 (entries 3.1–3.2 Table S3†). In contrast, 65% benzaldehyde conversion and a near quantitative yield (>99% selectivity) of the 2-methyl-5-[(5-methylfuran-2-yl)-phenylmethyl]furan (Scheme S2 and entry 3.3 Table S3†) HAA product was obtained at 65 °C after 1.5 h reaction. The turnover frequency (TOF) per acid site for Al-SBA-15 at 65 °C after 1.5 h reaction was ~24 h^{-1}. This value compares favourably with those reported for an acidic MOF[50] and Nafion-212 (ref. 51) of 8 h^{-1} and 25 h^{-1}, respectively, under similar reaction conditions. Rh/Al-SBA-15 was also active for HAA, exhibiting a small increase in conversion at the expense of selectivity to chain growth (entry 3.4 Table S3†), evidencing that precious metals are not required for HAA step. HAA of the crude product obtained from styrene hydroformylation (Table S2,† entry 2.1) was also attempted at 65 °C (entry 3.5). Complete conversion of both phenylpropanal isomers was observed with 90% selectivity to desired products **C** and **D**, confirming the effectiveness of Al-SBA-15 for step two of the cascade.

One-pot hydroformylation–HAA of styrene with 2-MF as reactant and solvent was then attempted at 80 °C and 30 bar CO/H_2. Without a catalyst, only 10% styrene conversion was observed with 66% selectivity to [**A** + **B**] (Table 2, entry 1) and no HAA products. In contrast, Rh/Al-SBA-15 achieved 98% conversion and 10% selectivity to the desired fuel precursors [**C** + **D**] (Table 2, entry 2). Negligible HAA occurred using 2-MF mixed with other solvents (Table S4†), consistent with literature reports.[52,53] However, longer reaction times (Table 2, entry 3) of 9 h only marginally improved the HAA product yield. As Al-SBA-15 was effective for HAA of the crude reaction mix from styrene hydroformylation in the absence of a CO/H_2 atmosphere (Table S3,† entry 3.5), we speculated that

Table 2 Cascade hydroformylation–HAA of styrene with 2-MF over Rh/Al-SBA-15

Entry	Solvent	CO/H_2/bar	Styrene conversion/%	Selectivity/%		
				A + **B**	**C** + **D**	Others[g]
1[a]	2-MF	30	10	66	—	34
2[b]	2-MF	30	98	80	10	10
3[c]	2-MF	30	100	60	15	25
4[d]	2-MF	30	100	04	60	36
5[d]	2-MF	20	82	08	67	25
6[d]	2-MF	10	25	12	63	25
7[e]	2-MF	30	91	05	09	86[h]
8[f]	2-MF	30	71	—	—	100[i]

Reaction conditions: [a] Blank. [b] 2.4 mmol styrene, 0.025 g 2.6 wt% Rh/Al-SBA-15, 16 mL 2-MF, 80 °C, 6 h. [c] As (b) but run for 9 h. [d] 2.4 mmol styrene, 0.025 g 2.6 wt% Rh/Al-SBA-15, 16 mL 2-MF, 80 °C, 6 h, then cooled to 60 °C and purged with N_2 prior to additional 3 h reaction. [e] As in (d) but cooled to 80 °C before N_2 purge. [f] Physical mixture of 0.025 g 2.6 wt% Rh/SBA-15 and 0.025 g Al-SBA-15, conditions as in (d). [g] Others mainly alkylbenzene and alkylation products. [h] Others mainly 2-methyl-5-(3-phenylprop-1-en-1-yl)furan. [i] Others mainly alkylated products. ^{13}C NMR of products **C** and **D** shown and mass spectrum of 2-methyl-5-(3-phenylprop-1-en-1-yl)furan formed in entry 7 are shown in Fig. S8.†

CO might chemisorb at Brønsted sites in the aluminosilicate support,[54] poisoning their HAA activity. A cascade reaction was therefore performed in which the initial hydroformylation reaction was allowed to proceed for 6 h over Rh/Al-SBA-15, after which CO/H_2 was purged from the reactor by N_2, and product analysis continued for a further 3 h. This protocol increased selectivity to [**C** + **D**] to 60% (Table 2, entry 4), indicating that the rate of HAA under a CO/H_2 atmosphere is approximately 10 times slower than under N_2.

Lower CO pressures led to decreased styrene conversion, but improved the selectivity for HAA (Table 2, entries 5–6), although this increase may also reflect suppressed styrene hydrogenation to ethyl benzene during the first step of the cascade. However, higher reaction temperature (Table 2, entry 7) led to poor HAA product yields, with dehydration of the monoalkylated intermediate favoured, producing 2-methyl-5-(3-phenylprop-1-en-1-yl)furan (Scheme S3†). Note that neither hydroformylation nor HAA products were observed in the absence of CO/H_2. Performing the tandem reaction with a physical mixture of Rh/SBA-15 and Al-SBA-15 (Table 2, entry 8) only led to byproducts of styrene oligomerisation and 2-MF alkylation. We attribute this observation to the poor hydroformylation activity of Rh/SBA-15 as previously reported in the literature where <20% aldehyde yield was obtained even at 100 °C.[55] We propose the excellent hydroformylation activity observed for Rh/Al-SBA-15 results from a strong synergy between the metal and support, potentially leading to

Table 3 Cascade hydroformylation–HAA of olefins with 2-MF over 2.6 wt% Rh/Al-SBA-15[a]

Entry	Substrate	Temperature/°C	Time/h	Conversion/%	Selectivity to fuel precursors (**C** + **D**)/%	Yield (**C** + **D**)/%	Other/%
1		80	9	>99	60	56	40
2[b]		80	9	100	80	79	20
3	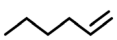	80	9	94	13	11	87
4	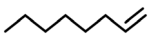	120	13	>99	23	20	77
5		80	9	50	40	38	60
6	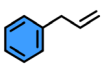	80	9	86	26	25	74
7	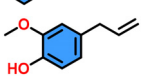	80	9	75	25	19	75
8	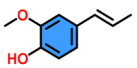	80	9	73	25	18	75

[a] Reaction conditions: 2.4 mmol of substrate and 10 wt% of catalyst to substrate dissolved in 16 mL of 2-methylfuran with CO/H_2 (1 : 1). After 6 h the reaction is cooled to 60 °C and purged with N_2 then pressurised to 20 bar and reaction continued for 3 h. [b] 5 bar propylene gas and 25 mg of catalyst dissolved in 16 mL of 2-methylfuran with 20 bar CO/H_2. Reaction cooled to 60 °C and CO/H_2 purged with N_2 after 6 h, then the reaction is carried out for 3 h under 20 bar N_2. ^{13}C and ^1H NMR for entry 1 and 6 shown in Fig. S9 and S10.† GC-MS for products shown in Fig. S11–S18.†

cooperative catalysis as reported for $Rh/WO_x/Al_2O_3$ (ref. 56) and Rh/siliceous MFI zeolite[57] catalysts wherein reaction proceeds by olefin adsorption on the support and spillover to metal sites. As discussed above, perturbation of the ^{27}Al MAS-NMR signal for Rh/Al-SBA-15 (Fig. 1d) may evidence a strong interaction between Rh and Al centres in Al-SBA-15 that facilitates such a synergy.

The versatility of Rh/Al-SBA-15 for the cascade hydroformylation–HAA of aliphatic and cyclic olefins was subsequently explored (Table 3). High olefin conversion was observed for propylene, 1-hexene and 1-octene, however only propylene delivered high selectivity (80%) to the desired long chain products (Table 3, entry 2). The low selectivity for 1-hexene and 1-octene reflects their isomerisation in competition with hydroformylation. Cyclohexene was less reactive (50% conversion) but afforded 40% selectivity to fuel range precursors (Table 3, entry 5), whereas <73% conversion was observed for allyl benzene, (bio-derived) eugenol and isoeugenol but with only 25% selectivity to desired products (Table 3, entries 6–8). For eugenol, the hydrogenated product was also observed whereas isoeugenol was stable to hydrogenation.

To our knowledge, the cascade hydroformylation–HAA of olefins is only previously reported for propene, 1-hexene and 1-octene using a $Rh(CO)_2(acac)$ homogeneous catalyst in conjunction with an AlOOH/C solid acid.[36] The present entirely heterogeneous catalyst system achieves a comparable yield of fuel precursor (79%) to that in our previous work (87%, for a combination of homogeneous and heterogeneous catalysts in addition to phosphine ligands).

Stability of the 2.6 wt% Rh/Al-SBA-15 catalyst was investigated through recycling reactions for the cascade hydroformylation–HAA of styrene with 2-MF at 80 °C and 20 bar (Fig. S5†). Styrene conversion fell to 49% on the first recycle, accompanied by a halving of selectivity to [**C** + **D**]. However, 550 °C calcination of the post-reaction catalyst to remove organic residues almost fully restored the initial activity and selectivity to their values for the parent catalyst (Table 2, entry 5). This regeneration protocol enabled the catalyst to be reused four times with only a 16% loss in conversion and 7% loss in selectivity relative to the as-prepared catalyst; equating to a decrease in the [**C** + **D**] yield from 56% to 40%. Surface analysis of the as-prepared catalyst and that recovered after four recycles confirmed a large increase in carbon (from 6.7 to 15 atom%, Table S5†) and the appearance of IR bands at 1465 and 1374 cm^{-1} assigned to $-CH_2$ and $-CH_3$ stretches, respectively (Fig. S6†),[57] accounting for the slight loss in reactivity. The apparent loss of Rh from XPS is attributed to the presence of carbonaceous residues capping the surface of the metal nanoparticles, and concomitant attenuation of the Rh XP signal. TGA of the as-prepared catalyst under flowing air revealed a ~5 wt% loss between 25–100 °C (Fig. S19†) attributed to physisorbed water, and a further ~8 wt% loss due to dehydration of geminal and vicinal silanols (to siloxanes) between 100–250 °C. Post-reaction (after one reaction cycle under the optimum conditions) revealed a significant mass loss >310 °C associated with combustion of organic residues that accounted for ~15–20 wt% of the catalyst mass.

Many ligand-free nanoparticulate Rh catalysts suffer severe deactivation after one reaction cycle due to metal leaching.[12] The reusability of Rh/Al-SBA-15 thus meets an important requirement for the present one-pot, two-step hydroformylation and HAA of olefins. Furthermore, the thermal stability of Al-SBA-15 offers advantages over organic solid acids often used for HAA such as sulfonic acid functionalised carbon[29] and silica,[58] acidic MOFs[50] or polymer based catalysts *e.g.* Nafion[59] or sulfonated resins[60] that are difficult to thermally regenerate to remove reaction residues. The strong synergy between Rh and Al-SBA-15 promotes hydroformylation compared to Rh/SBA-15,[55,61] and will require future mechanistic and operando studies to identify the nature of the active Rh species. Increasing the metal dispersion to the limit of single atoms could yield further improvements as Rh single atom catalysts are highly active for hydroformylation, *e.g.* 0.006 wt% Rh/ZnO nanowires exhibit a quantitative yield of aldehydes and high TON at 100 °C.[62] Further studies will also explore the loading dependence of Rh-Al-SBA-15 to determine whether highly active single atom Rh centres can be stabilised in the defective Al-SBA-15 surface as was previously observed for Pd catalysts.[63]

Considering commercial application, the relatively low value and volume demand of sustainable aviation fuel compared to specialty chemicals will necessitate a continuous process to be economically viable, as for other global scale acid-metal bifunctional catalytic processes.[64] Cascading hydroformylation and HAA reactions in a single continuous reactor over Rh/Al-SBA-15 may prove uneconomic due to inhibition of the latter by syngas; this would necessitate frequent reactor (de)pressurisation/purging cycles. A three unit continuous process in which the two reactions are decoupled may thus be envisaged involving: (i) three-phase hydroformylation of alkenes over Rh/Al-SBA-15, possibly in a continuous stirred-tank reactor; (ii) transfer of the liquid aldehyde product and unreacted syngas to a gas–liquid separation unit; and (ii) mixing of the liquid aldehyde stream with 2-MF and transfer into a second continuous stirred-tank reactor containing an Al-SBA-15 catalyst. Periodic catalyst regeneration (through calcination) could be achieved by adopting a chemical looping approach in which the alkene/syngas feed is temporarily switched for an oxygen/air stream.[65] We note that multifunctional catalysts that permit one-pot reactions are not always advantageous *versus* separate catalysts in multiple connected reactors, *e.g.* the cascade conversion of lauric acid to tricosane (as a route to renewable diesel)[66] and the cascade selective oxidation of cinnamyl alcohol to cinnamic acid[67] are more efficient using contiguous, dual-catalyst packed beds.

Conclusions

In summary, Rh/Al-SBA-15 is an effective catalyst for the one-pot batchwise synthesis of jet and diesel fuel precursors from olefins and 2-MF through a hydroformylation–HAA cascade. Use of an entirely heterogeneous catalyst obviates the need for costly P- or N-organic ligands, previously required to drive the cascade with homogeneous Rh catalysts, and minimises precious metal losses. A range of aliphatic and cyclic olefins are amenable to this cascade, which for styrene yields 56% of the desired fuel precursors under relatively mild conditions of 80 °C and 30 bar CO/H_2 in 9 h. Although the HAA step is poisoned by high pressures of CO, this issue is readily addressed by purging syngas from the reactor after the initial hydroformylation is completed. Unreacted syngas could be recovered and reused. Rh/Al-SBA-15 is susceptible to gradual poisoning by the accumulation organic residues but can be repeatedly regenerated by calcination for at least five reaction cycles. Future research will explore continuous processing for reaction optimisation, permitting the hydroformylation and hydroxyalkylation steps to run simultaneously in separate metal and acid catalyst beds at different temperatures, with the continuous recovery and reuse of unreacted syngas.

Data availability

The data supporting this article have been included as part of the ESI.†

Conflicts of interest

There are no conflicts to declare.

Acknowledgements

K. R. acknowledges CSIR, Govt. of India, for the Senior Research Fellowship (CSIR Grant No.: 31/028(0253)/2019-EMR-I). H. K. acknowledges CSIR, Govt. of India, for the Senior Research Fellowship (CSIR Grant No.: 31/0028(11360)/2021-EMR-I). A. V. B. acknowledges the Science & Engineering Research Board (SERB/CRG/2022/001857), India, for financial support. The Analytical and Environmental Science Division and Centralized Instrumentation Facility of CSIR-Central Salt & Marine Chemicals and Research Institute, Bhavnagar, is acknowledged for providing all requisite instrumental analysis. K. W. and A. F. L. acknowledge funding from the Australian Research Council (DP200100204, DP200100313, and LP190100849). We also acknowledge the insightful comments from the reviewer in suggesting points for consideration regarding the practical application of this process for fuel production.

Notes and references

1 M. J. Climent, A. Corma and S. Iborra, *Chem. Rev.*, 2011, **111**, 1072–1133.
2 K. Lee, Y. Jing, Y. Wang and N. Yan, *Nat. Rev. Chem.*, 2022, **6**, 635–652.
3 *IPCC, 2022: Summary for Policymakers*, ed. J. S. P. R. Shukla, R. Slade, A. Al Khourdajie, R. van Diemen, D. McCollum, M. Pathak, S. Some, P. Vyas, R. Fradera, M. Belkacemi, A. Hasija, G. Lisboa, S. Luz and J. Malley, Cambridge University Press, Cambridge, UK and New York, NY, USA, 2022.
4 S. Voelker, N. Groll, M. Bachmann, L. Mueller, M. Neumann, T. Kossioris, P. Muthyala, B. Lehrheuer, M. Hofmeister, A. Vorholt, K. Schmitz, S. Pischinger, W. Leitner and A. Bardow, *Nat. Energy*, 2024, **9**, 1220–1229.
5 S. Püschel, S. Störtte, J. Topphoff, A. J. Vorholt and W. Leitner, *ChemSusChem*, 2021, **14**, 5226–5234.
6 H. Li, J. Wu, Z. Jiang, J. Ma, V. M. Zavala, C. R. Landis, M. Mavrikakis and G. W. Huber, *Science*, 2023, **381**, 660–666.
7 M. Mascal, *Biofuels, Bioprod. Biorefin.*, 2012, **6**, 483–493.
8 J. L. Grant, C. H. Hsieh and T. M. Makris, *J. Am. Chem. Soc.*, 2015, **137**, 4940–4943.
9 C. M. Simon, W. Kaminsky and B. Schlesselmann, *J. Anal. Appl. Pyrolysis*, 1996, **38**, 75–87.
10 R. Franke, D. Selent and A. Börner, *Chem. Rev.*, 2012, **112**, 5675–5732.
11 B. Liu, Y. Wang, N. Huang, X. Lan, Z. Xie, J. G. Chen and T. Wang, *Chem*, 2022, **8**, 2630–2658.
12 S. Alini, A. Bottino, G. Capannelli, A. Comite and S. Paganelli, *Appl. Catal., A*, 2005, **292**, 105–112.
13 X. Li, T. Qin, L. Li, B. Wu, T. Lin and L. Zhong, *Catal. Lett.*, 2021, **151**, 2638–2646.
14 M.-L. Kontkanen, M. Tuikka, N. M. Kinnunen, S. Suvanto and M. Haukka, *Catalysts*, 2013, **3**, 324–337.
15 T. Li, F. Chen, R. Lang, H. Wang, Y. Su, B. Qiao, A. Wang and T. Zhang, *Angew. Chem., Int. Ed.*, 2020, **59**, 7430–7434.
16 M. Tan, Y. Ishikuro, Y. Hosoi, N. Yamane, P. Ai, P. Zhang, G. Yang, M. Wu, R. Yang and N. Tsubaki, *Chem. Eng. J.*, 2017, **330**, 863–869.
17 T. V. Vu, H. Kosslick, A. Schulz, J. Harloff, E. Paetzold, H. Lund, U. Kragl, M. Schneider and G. Fulda, *Microporous Mesoporous Mater.*, 2012, **154**, 100–106.
18 D. Sharma, V. Ganesh and A. Sakthivel, *Appl. Catal., A*, 2018, **555**, 155–160.
19 E. Vunain, P. Ncube, K. Jalama and R. Meijboom, *J. Porous Mater.*, 2018, **25**, 303–320.
20 Q. Sun, Z. Dai, X. Liu, N. Sheng, F. Deng, X. Meng and F.-S. Xiao, *J. Am. Chem. Soc.*, 2015, **137**, 5204–5209.
21 C. Li, K. Sun, W. Wang, L. Yan, X. Sun, Y. Wang, K. Xiong, Z. Zhan, Z. Jiang and Y. Ding, *J. Catal.*, 2017, **353**, 123–132.
22 S. Feng, Q. Yu, X. Ma, X. Yu and N. Yan, *National Science Open*, 2023, **2**, 20220064.
23 J. Liu, L. Yan, Y. Ding, M. Jiang, W. Dong, X. Song, T. Liu and H. Zhu, *Appl. Catal., A*, 2015, **492**, 127–132.
24 R. Xing, A. V. Subrahmanyam, H. Olcay, W. Qi, G. P. van Walsum, H. Pendse and G. W. Huber, *Green Chem.*, 2010, **12**, 1933–1946.
25 A. V. Subrahmanyam, S. Thayumanavan and G. W. Huber, *ChemSusChem*, 2010, **3**, 1158–1161.

26 H. Zang and E. Y. X. Chen, *Int. J. Mol. Sci.*, 2015, **16**, 7143–7158.
27 J. S. Kwon, H. Choo, J.-W. Choi, J. Jae, D. Jin Suh, K. Young Lee and J.-M. Ha, *Appl. Catal., A*, 2019, **570**, 238–244.
28 K. Ravi and A. V. Biradar, *Fuel*, 2022, **321**, 124008.
29 Y. Zhong, P. Zhang, X. Zhu, H. Li, Q. Deng, J. Wang, Z. Zeng, J.-J. Zou and S. Deng, *ACS Sustainable Chem. Eng.*, 2019, **7**, 14973–14981.
30 R. Zhong, Y. Liao, R. Shu, L. Ma and B. F. Sels, *Green Chem.*, 2018, **20**, 1345–1353.
31 Q. Deng, P. Han, J. Xu, J.-J. Zou, L. Wang and X. Zhang, *Chem. Eng. Sci.*, 2015, **138**, 239–243.
32 A. Kunamalla and S. K. Maity, *Fuel*, 2023, **332**, 125977.
33 Y. Tan, Y. Li, Y. Wei, Z. Wu, J. Yan, L. Pan and Y. Liu, *Catal. Commun.*, 2015, **67**, 21–25.
34 A. Shivhare, J. A. Hunns, L. J. Durndell, C. M. A. Parlett, M. A. Isaacs, A. F. Lee and K. Wilson, *ChemSusChem*, 2020, **13**, 4945–4953.
35 K. B. Baharudin, M. Arumugam, J. Hunns, A. F. Lee, E. Mayes, Y. H. Taufiq-Yap, K. Wilson and D. Derawi, *Catal.: Sci. Technol.*, 2019, **9**, 6673–6680.
36 K. Ravi, A. F. Lee, K. Wilson and A. V. Biradar, *ACS Sustainable Chem. Eng.*, 2024, **12**, 1632–1644.
37 A. Corma, O. de la Torre and M. Renz, *Energy Environ. Sci.*, 2012, **5**, 6328–6344.
38 C. Schlumberger and M. Thommes, *Adv. Mater. Interfaces*, 2021, **8**, 2002181.
39 Z. Xue, H. Shang, Z. Zhang, C. Xiong, C. Lu and G. An, *Energy Fuels*, 2017, **31**, 279–286.
40 K. B. Baharudin, Y. H. Taufiq-Yap, J. Hunns, M. Isaacs, K. Wilson and D. Derawi, *Microporous Mesoporous Mater.*, 2019, **276**, 13–22.
41 J. M. R. Gallo, C. Bisio, G. Gatti, L. Marchese and H. O. Pastore, *Langmuir*, 2010, **26**, 5791–5800.
42 L. S. Kibis, A. I. Stadnichenko, S. V. Koscheev, V. I. Zaikovskii and A. I. Boronin, *J. Phys. Chem. C*, 2016, **120**, 19142–19150.
43 Y. Kwon, T. Y. Kim, G. Kwon, J. Yi and H. Lee, *J. Am. Chem. Soc.*, 2017, **139**, 17694–17699.
44 A. B. Kroner, M. A. Newton, M. Tromp, A. E. Russell, A. J. Dent and J. Evans, *ChemPhysChem*, 2013, **14**, 3606–3617.
45 C. T. Williams, K. Y. Chen, C. G. Takoudis and M. J. Weaver, *J. Phys. Chem. B*, 1998, **102**, 4785–4794.
46 M. Gómez-Cazalilla, J. M. Mérida-Robles, A. Gurbani, E. Rodríguez-Castellón and A. Jiménez-López, *J. Solid State Chem.*, 2007, **180**, 1130–1140.
47 J.-C. Dupin, D. Gonbeau, P. Vinatier and A. Levasseur, *Phys. Chem. Chem. Phys.*, 2000, **2**, 1319–1324.
48 A. L. Watkins and C. R. Landis, *J. Am. Chem. Soc.*, 2010, **132**, 10306–10317.
49 S. Liu, X. Dai, H. Wang, X. Wang and F. Shi, *Chin. J. Chem.*, 2020, **38**, 139–143.
50 E. C. Atayde, B. M. Matsagar, Y.-C. Wang and K. C. W. Wu, *Appl. Catal., A*, 2024, **669**, 119492.
51 G. Li, N. Li, J. Yang, A. Wang, X. Wang, Y. Cong and T. Zhang, *Bioresour. Technol.*, 2013, **134**, 66–72.
52 Q. Xia, Y. Xia, J. Xi, X. Liu, Y. Zhang, Y. Guo and Y. Wang, *ChemSusChem*, 2017, **10**, 747–753.
53 S. Dutta, A. Bohre, W. Zheng, G. R. Jenness, M. Núñez, B. Saha and D. G. Vlachos, *ACS Catal.*, 2017, **7**, 3905–3915.
54 F. Leydier, C. Chizallet, D. Costa and P. Raybaud, *Chem. Commun.*, 2012, **48**, 4076–4078.
55 M. Chen, G. Gupta, C. W. Ordonez, A. R. Lamkins, C. J. Ward, C. A. Abolafia, B. Zhang, L. T. Roling and W. Huang, *J. Am. Chem. Soc.*, 2021, **143**, 20907–20915.
56 I. Ro, J. Qi, S. Lee, M. Xu, X. Yan, Z. Xie, G. Zakem, A. Morales, J. G. Chen, X. Pan, D. G. Vlachos, S. Caratzoulas and P. Christopher, *Nature*, 2022, **609**, 287–292.
57 Y. Liu, Z. Liu, Y. Hui, L. Wang, J. Zhang, X. Yi, W. Chen, C. Wang, H. Wang, Y. Qin, L. Song, A. Zheng and F.-S. Xiao, *Nat. Commun.*, 2023, **14**, 2531.
58 M. S. Zanuttini, L. G. Tonutti, C. A. Neyertz, C. Ferretti, B. S. Sánchez, B. O. Dalla Costa and C. A. Querini, *Appl. Catal., A*, 2023, **665**, 119383.
59 G. Ren, G. Li, Y. Zhang, A. Wang, X. Wang, Y. Cong, T. Zhang and N. Li, *Sustainable Energy Fuels*, 2022, **6**, 1156–1163.
60 X. Zhang, Q. Deng, P. Han, J. Xu, L. Pan, L. Wang and J.-J. Zou, *AIChE J.*, 2017, **63**, 680–688.
61 L. Zhu, C. Li, Q. Yun, S. Han, Y. Lv, Q. Lu and J. Chen, *Chin. Chem. Lett.*, 2023, **34**, 108515.
62 R. Lang, T. Li, D. Matsumura, S. Miao, Y. Ren, Y.-T. Cui, Y. Tan, B. Qiao, L. Li, A. Wang, X. Wang and T. Zhang, *Angew. Chem., Int. Ed.*, 2016, **55**, 16054–16058.
63 S. F. J. Hackett, R. M. Brydson, M. H. Gass, I. Harvey, A. D. Newman, K. Wilson and A. F. Lee, *Angew. Chem., Int. Ed.*, 2007, **46**, 8593–8596.
64 M. J. Climent, A. Corma, S. Iborra and M. J. Sabater, *ACS Catal.*, 2014, **4**, 870–891.
65 A. Oing, E. von Müller, F. Donat and C. R. Müller, *Energy Fuels*, 2024, **38**, 17326–17342.
66 A. Corma, M. Renz and C. Schaverien, *ChemSusChem*, 2008, **1**, 739–741.
67 L. J. Durndell, M. A. Isaacs, C. e. Li, C. M. A. Parlett, K. Wilson and A. F. Lee, *ACS Catal.*, 2019, **9**, 5345–5352.

